NASA Technical Memorandum

NASA TM-86474

OPTICAL ANALYSIS OF THE STAR-TRACKER TELESCOPE FOR GRAVITY PROBE

By D. E. Zissa

Information and Electronic Systems Laboratory

October 1984

NASA
National Aeronautics and Space Administration

George C. Marshall Space Flight Center

TABLE OF CONTENTS

LIST OF ILLUSTRATIONS

LIST OF TABLES

TECHNICAL MEMORANDUM

OPTICAL ANALYSIS OF THE STAR-TRACKER TELESCOPE FOR GRAVITY PROBE

I. INTRODUCTION

An extremely precise star tracker is needed for attitude control and angular reference. At MSFC, ray trace modeling of the Stanford optical design has been used to predict the character of the output signal and its sensitivity to fabrication errors. Photomultiplier and solid state detector options were considered. The results were compared with requirements and recommendations were made.

II. DESCRIPTION OF THE STAR-TRACKER

A. Requirements

The star-tracker requirements stated in the Stanford report [1] are reproduced here:

1) Independent readout of angular position in two planes, orthogonal to each other and aligned with the gyro readout planes to within a few arc-sec.

2) Absolute null stability over a one-year period of mechanical parts and readout to 1 milliarc-sec.

3) Readout linear to 1 milliarc-sec over ±0.05 arc-sec, and having an acquisition range of ±2 arc-min.

4) Noise performance leading to a resolution of 0.05 arc-sec in 0.1 sec observation time of the chosen reference star (probably Rigel), and capable of integration to 0.001 arc-sec over a longer period.

5) Provision for automatic gain control, referred to the gyroscope, capable of matching the gains of the gyroscope and telescope readouts to 1 percent or better.

The primary concern of this study was the impact of the optical subsystem on the linearity requirement stated in item (3). Extreme linearity would minimize the amount of calibration needed. Although the study emphasized item (3), the results are applicable to (2) and (4).

B. Stanford Optical Design

The Stanford optical prescription [1] shown in Figure 1 may roughly be described as a folded Schmidt-Cassegrain design. The use of all spherical mirrors requires a corrector plate to obtain a diffraction limited spot size. The entrance aperture is 2.8 in. in radius and the radius is half obscured. The effective focal length is 150 in. The image plane is approximately 1 in. in front of the corrector plate. The physical length of the telescope is about 14 in.

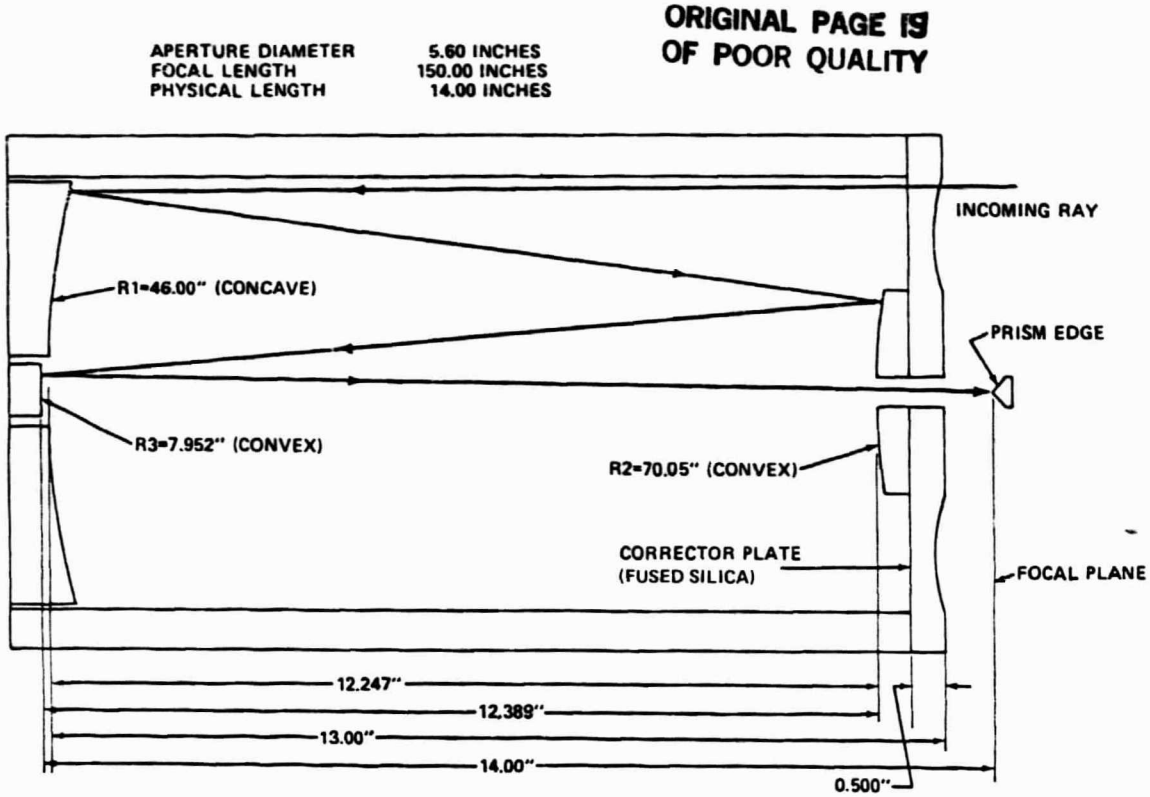

Figure 1. Schematic of telescope optics.

The output signal would be developed as follows: A beam splitter directs an image spot onto each of two prism edges. In this way an image divider is set up for motion in two orthogonal directions. Then light from either side of an image divider is alternately directed by a mechanical light chopper to the same place on the photocathode of a photomultiplier tube. (Otherwise differential aging of the photocathode surface would cause problems.) The output signal is proportional to the difference between photomultiplier outputs resulting from the light on either side of the dividing edge. Note that the combined actions of the beam splitter and mechanical chopper, cut the effective light intensity by a factor of 4.

C. CID Detector Option

A charge injection device [2], CID, could possibly replace the beam splitter, prism edges, mechanical light choppers, and photomultiplier tubes. The CID is a square array of solid-state pixels each approximately 20 microns square. The image divider would be a boundary between detector pixels. For the present analysis the differences calculated for the output signal were due to differences in the quantum efficiency spectrum of the detector systems considered.

Two advantages of the particular wide-band CID considered here are greater quantum efficiency and larger average wavelength. Also, there would be no moving parts. A possible disadvantage is that the detailed image must be preserved up to the detector surface, possibly by a fiber optic bundle. Another consideration would be the quality of image division by a pixel boundary.

III. ANALYSIS PROCEDURE

A. Telescope Model

The optical elements included for the ray-trace modeling were a corrector plate, three spherical mirrors, and a perfect image divider at the focus. It was assumed that the telescope would pass the effective spectrum of star and detector with a flat optical power efficiency of 10 percent. There was an additional factor of 25 percent where the photomultiplier was used with the beam splitter and choppers.

The specific detectors used in the model were the S20 photomultiplier tube [3] and a wide band CID, the General Electric ST256 1-12-23 [2].

B. Effective Spectral Flux from Rigel

The proposed guide star Rigel was treated as a black body at 12,203°K with an apparent visual magnitude of 0.11 [4]. The effective spectral flux was calculated by multiplying Rigel's spectral flux by the quantum efficiency for each detector. Figure 2 shows quantum efficiency and effective spectral flux for the S20 and CID options not including the 10 percent and 25 percent efficiencies mentioned in IIIA.

C. Calculation of Image Spot Intensity Distribution or Point Spread Function (PSF)

First, parallel rays on a 70 x 70 rectangular grid at the entrance pupil were followed to the exit pupil by means of an exact ray trace [5]. Then a Fourier transform operation on the exit pupil wavefront gave the image amplitude, the square of which is the image intensity distribution or PSF. The net PSF was the weighted sum of ten PSF's over the effective spectrum of Rigel and detector.

D. Calculation of the Output Signal and Its Deviation from Linearity

The raw output signal was obtained as the difference between the detected photon rate (photons/sec) on either side of a line that was moved through the effective image spot. The signal was scaled to arc-seconds by the average slope of the raw signal versus angular displacement within ±10 milliarc-sec of the null point. The linearity deviations reported below are the differences between the signal and a straight line tangent to the signal curve at the null point. Although this is a good measure of the deviations of the output signal from a straight line, this is not necessarily the best way to process the signal during operation of the spacecraft. For example, the signal may be scaled by the average slope over ±30 milliarc-sec about the null point.

For calculation of the linearity deviations in the central ±110 milliarc-sec range, the PSF was calculated on a grid with 7.3 μ-in. (10 milliarc-sec) intervals. The computational accuracy of the linearity deviations is about 0.1 and 0.2 milliarc-sec at ±50 milliarc-sec and ±110 milliarc-sec, respectively.

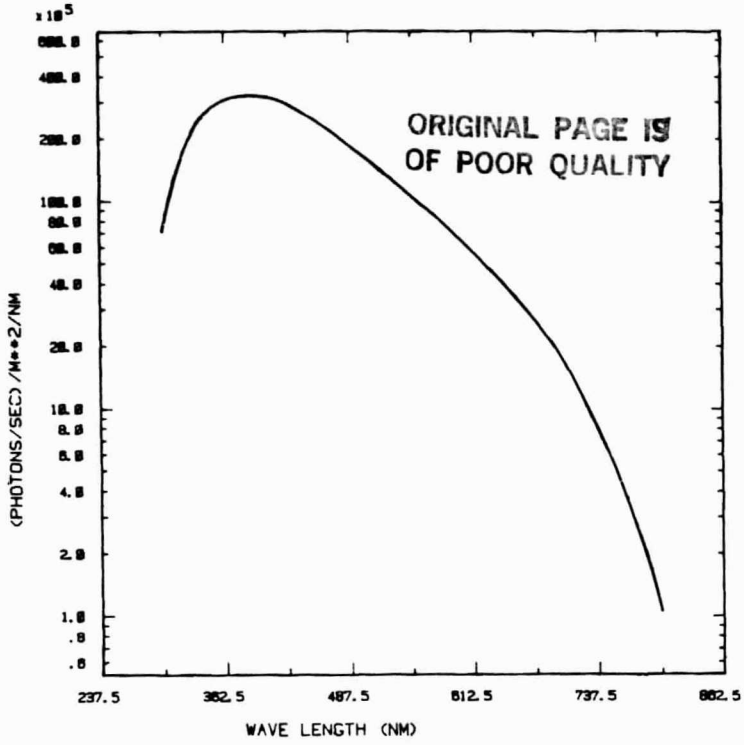

Figure 2a. Effective spectral flux, Rigel to S20 (see Section III-b).

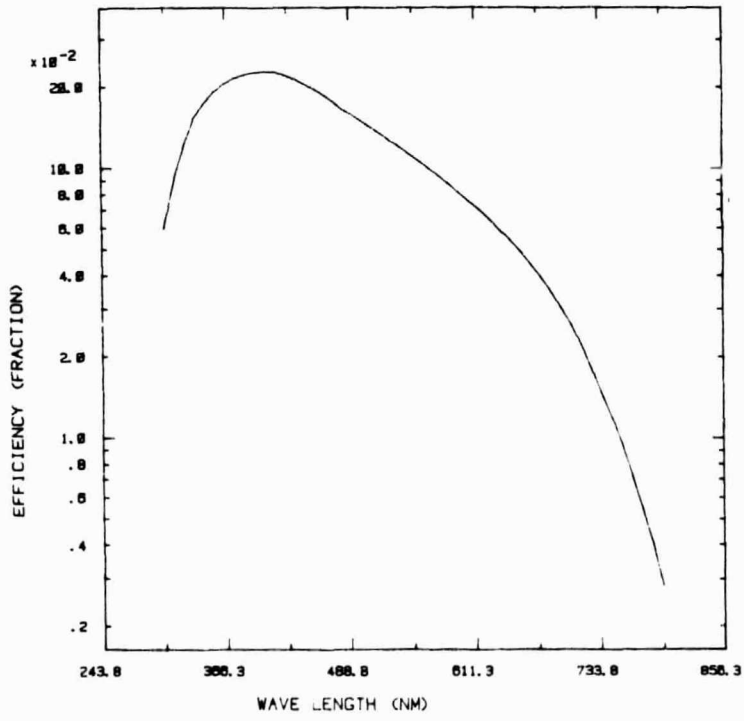

Figure 2b. Quantum efficiency of S20.

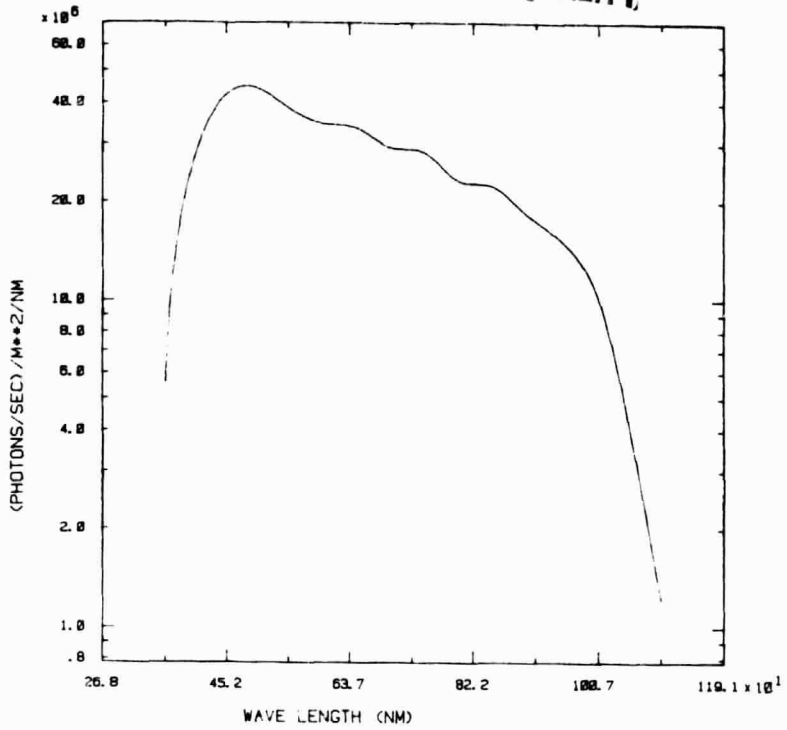

Figure 2c. Effective spectral flux, Rigel to CID (see Section III-B).

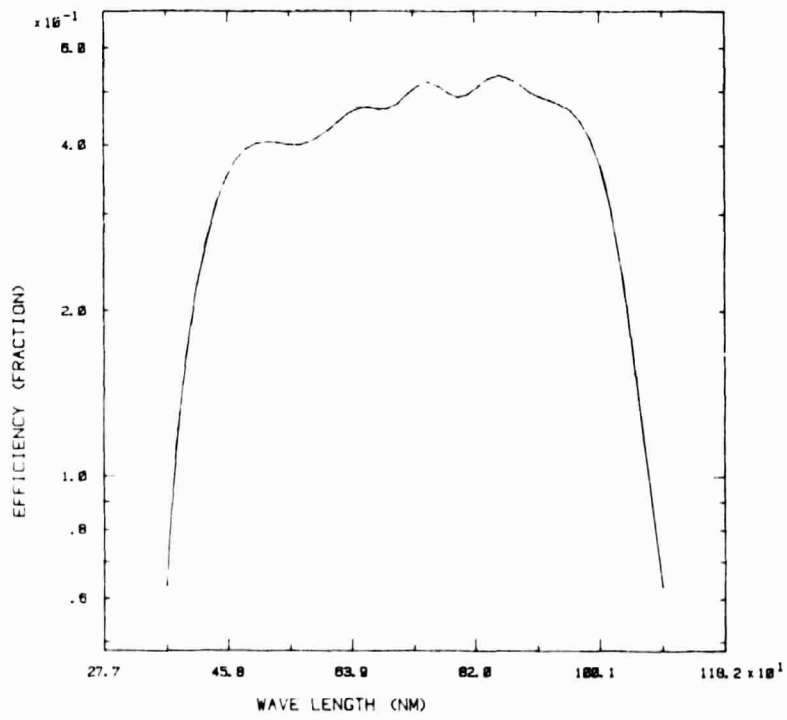

Figure 2d. Quantum efficiency of CID.

IV. NOMINAL CHARACTERISTICS

A. PSF

Figure 3 shows the normalized PSF shapes calculated from the telescope model with both detectors. The wide band CID "sees" a larger spot since it is more sensitive to longer wavelengths. (Spot size is proportional to λ/D where λ and D are the wavelength and aperture diameter, respectively). Statistics on the PSF and resulting signal are shown in Table 1. The calculated effective photon rates for this wide band CID are an order of magnitude larger than those of the S20 version.

B. Output Signal and Linearity Deviation

Figure 4 shows the calculated nominal output signal. Figure 5 shows the resulting linearity deviations within ±110 milliarc-sec of the null point. The maximum deviations within ±50 milliarc-sec and ±110 milliarc-sec are shown in Table 2. The wide-band CID option would be more linear due to the large spot size.

C. Noise Equivalent Angle (NEA)

Statistical fluctuation in the photon arrival rate contributes to the noise in the output signal. The rms error from this source was calculated to be ±1.1 and ±0.5 milliarc-sec for the S20 and CID, respectively, for 0.1 sec time integration. The figure is larger for the S20 version because the detected photon rate is smaller. However, both values were much smaller than the stated requirements.

V. SENSITIVITY TO FABRICATION ERRORS

A. Random Surface Error

The effect of random surface error of the optical elements was studied by adding random error to the wavefront. The effect depends both on the magnitude and correlation length of the wavefront error. The two dimensional random error function was smoothed by a Gaussian shape such that there were about 5 "bumps" per exit pupil diameter. Figure 6 shows sample PSF shapes with $\lambda/20$ and $\lambda/40$ rms random wavefront errors where λ = 632.8 nm. Figure 7 shows sample linearity deviation curves in two orthogonal directions from 10 such trials with $\lambda/20$ and $\lambda/40$ rms random wavefront errors. The maximum deviations within ±50 milliarc-sec and ±110 milliarc-sec are tabulated in Table 2.

B. Image Divider Defects

A long "chip" which extends alongside the image dividing line to the center of the image spot and which "reflects" light to the opposite side of the image divider would have a maximal effect on linearity. Movement along the dividing line would cause signal variation in the orthogonal direction. Deviation due to such a 5 μ-in.-wide chip over ±50 milliarc-sec could be as large as 1.1 and 0.8 milliarc-sec for the S20 and CID versions, respectively.

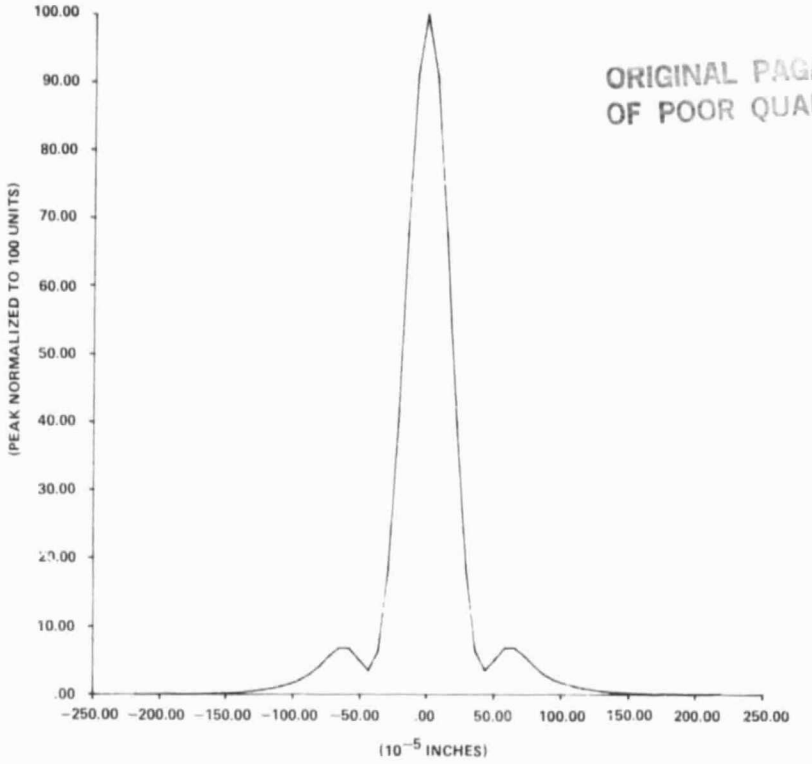

Figure 3a. Normalized PSF, Rigel to S20.

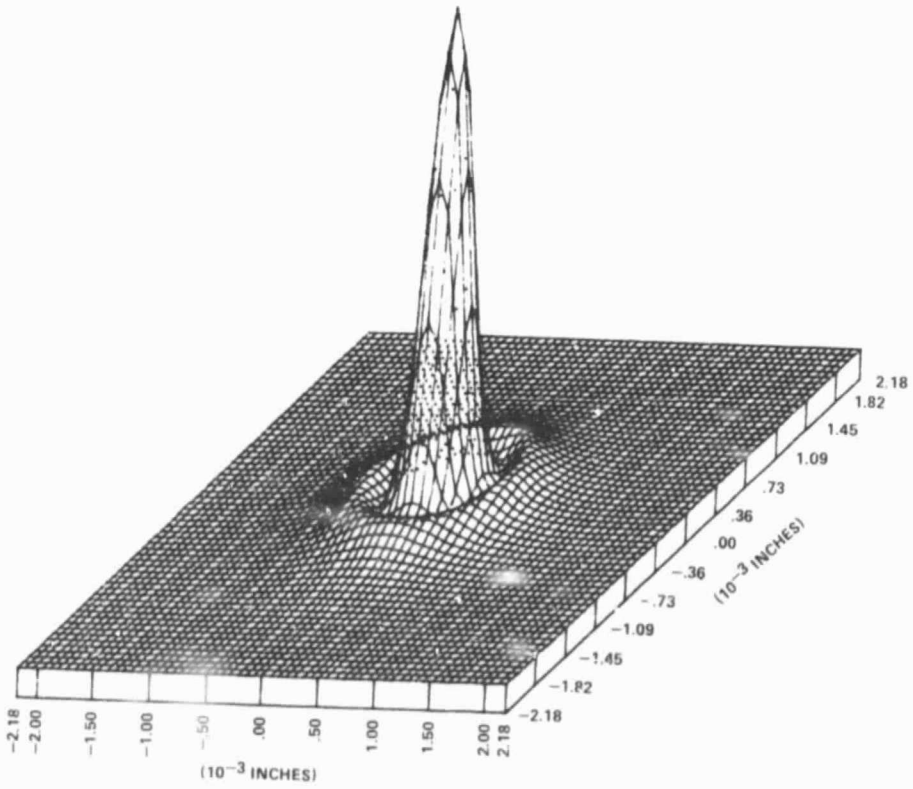

Figure 3b. Normalized PSF, Rigel to S20.

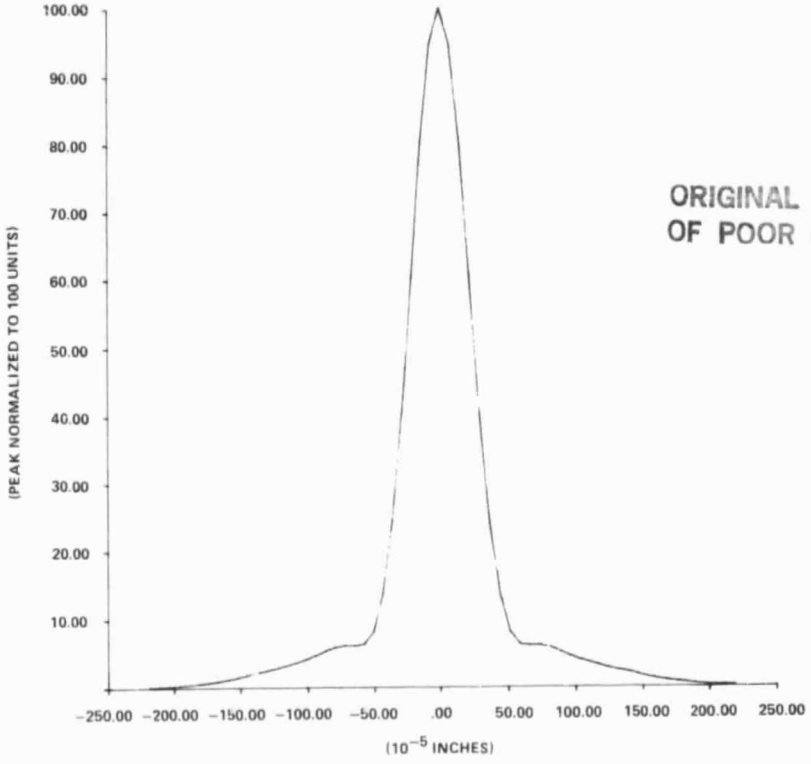

Figure 3c. Normalized PSF, Rigel to CID.

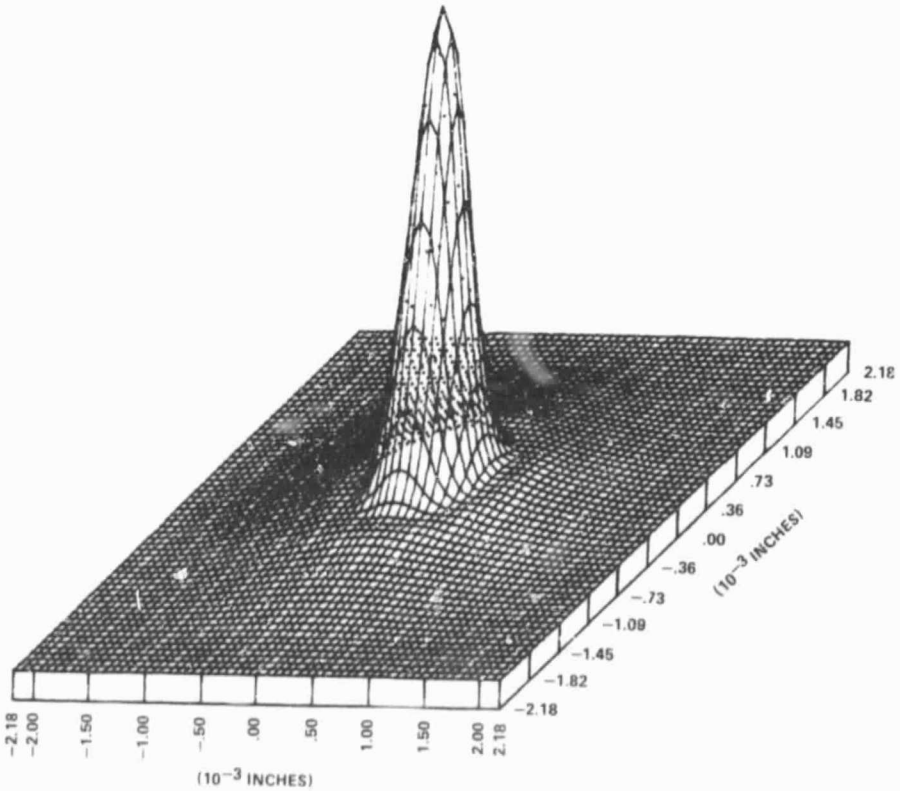

Figure 3d. Normalized PSF, Rigel to CID.

TABLE 1. SPECTRAL AND PSF STATISTICS FROM MODEL

	S20[a,b]	CID[b]
Average wavelength (nm)	442	650
Rms spectral width (nm)	91	175
Peak wavelength (nm)	385	485
Total spectral width (nm)	300-800	360-1100
Effective intensity of central maximum of PSF (photons/sec/in.^{2})	5.9×10^{12} (4.9×10^{11})[c]	3.4×10^{13} (9.8×10^{12})[c]
Total effective photon rate (photons/sec)	1.9×10^{6}	2.2×10^{7}
Sensitivity (photons/sec/milliarc-sec)	4.0×10^{3} (1.0×10^{3})[c]	3.2×10^{4} (1.5×10^{4})[c]

a. Factor of 0.25 applied to flux for beam splitter and chopper.
b. Factor of 0.10 applied to flux for optical efficiency of telescope.
c. Divider edge moved 0.1 in. from focus.

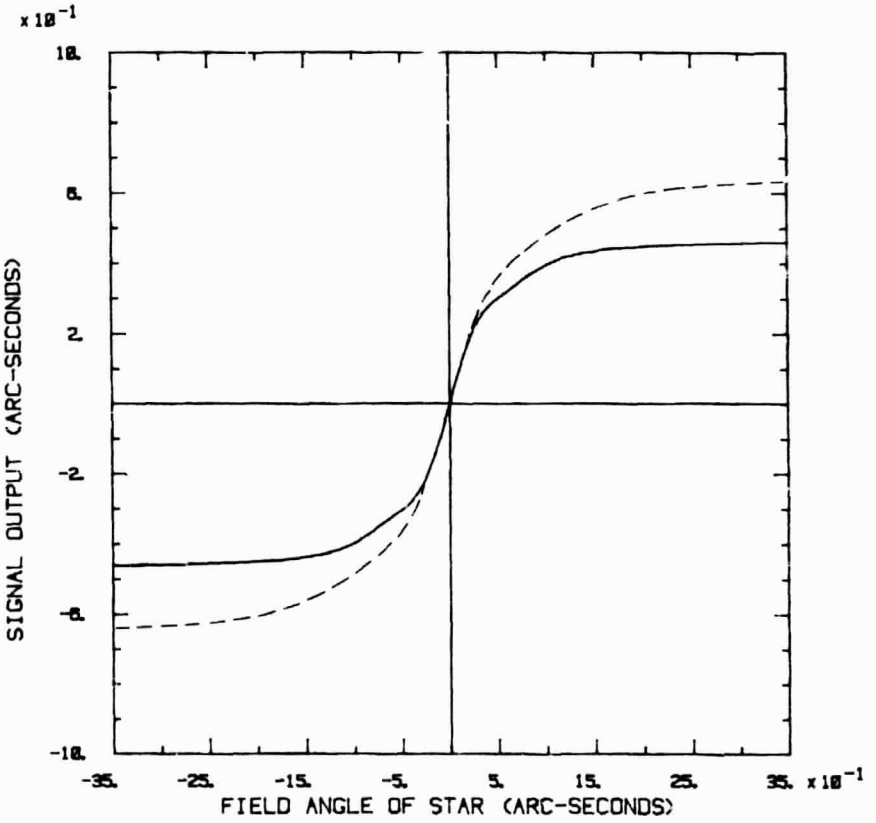

Figure 4. Nominal output signal: Rigel to S20 (solid curve), Rigel to CID (dashed curve).

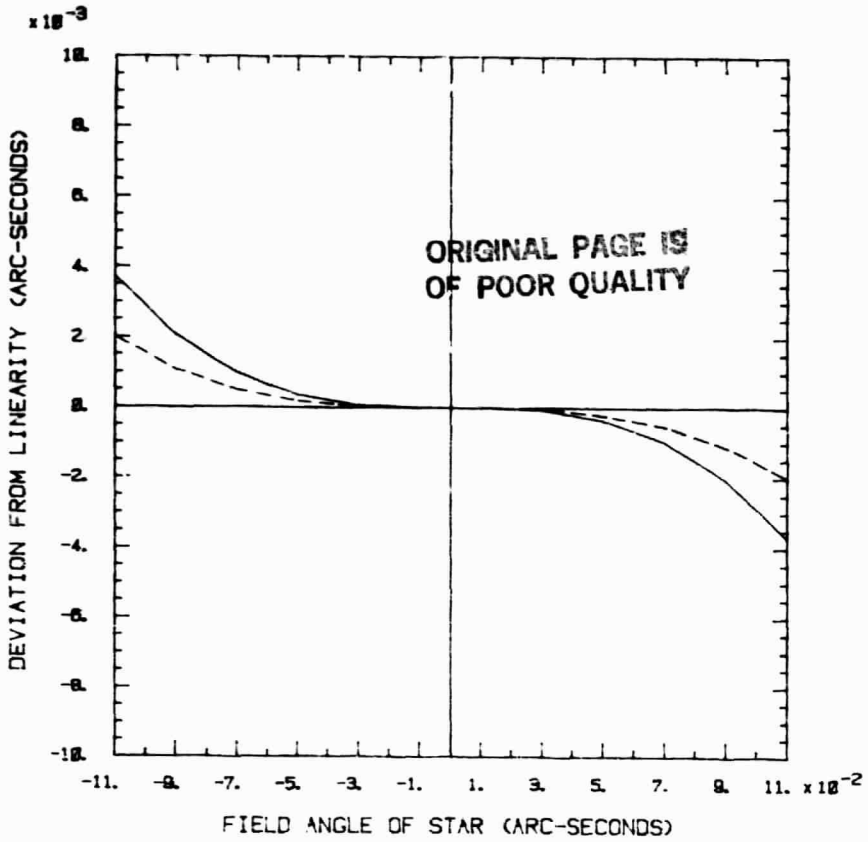

Figure 5. Linearity deviation with nominal signal: Rigel to S20 (solid curve), Rigel to CID (dashed curve).

TABLE 2. MAXIMUM DEIVATION FROM LINEARITY IN ±50 AND ±110 MILLIARC-SEC RANGES (UNITS: MILLIARC-SEC)

		S20	CID
Nominal	± 50	0.35	0.19
	±110	3.71	2.06
With λ/20 rms wavefront error[a,b]	± 50	1.2	0.7
	±110	7.3	4.2
With λ/40 rms wavefront error[a,b]	± 50	0.8	0.5
	±110	5.7	3.2

a. Random error smoothed with Gaussian shape such that there were about five "bumps" per exit pupil diameter.
b. Ten trials in two orthogonal directions.

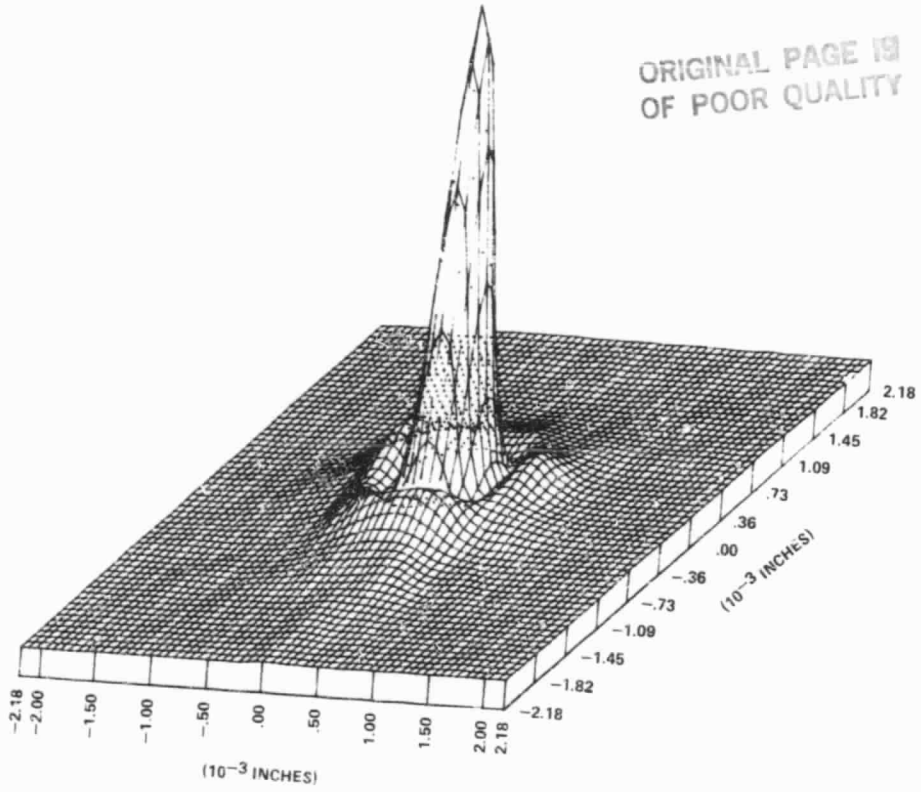

Figure 6a. Normalized PSF with $\lambda/20$ rms wavefront error, Rigel to S20.

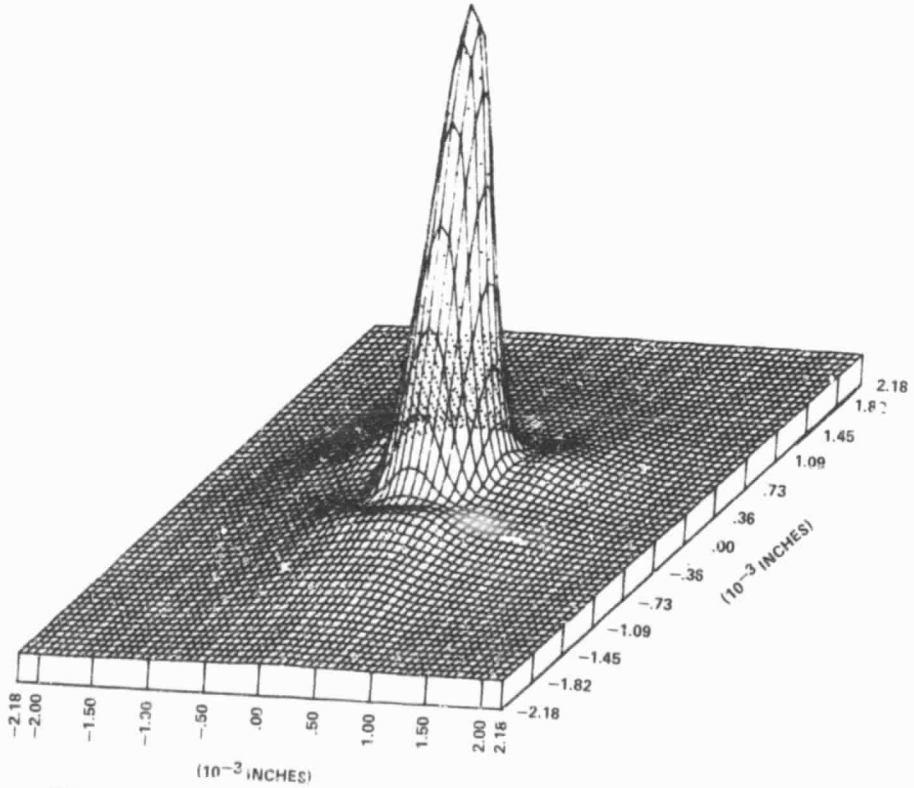

Figure 6b. Normalized PSF with $\lambda/20$ rms wavefront error, Rigel to CID.

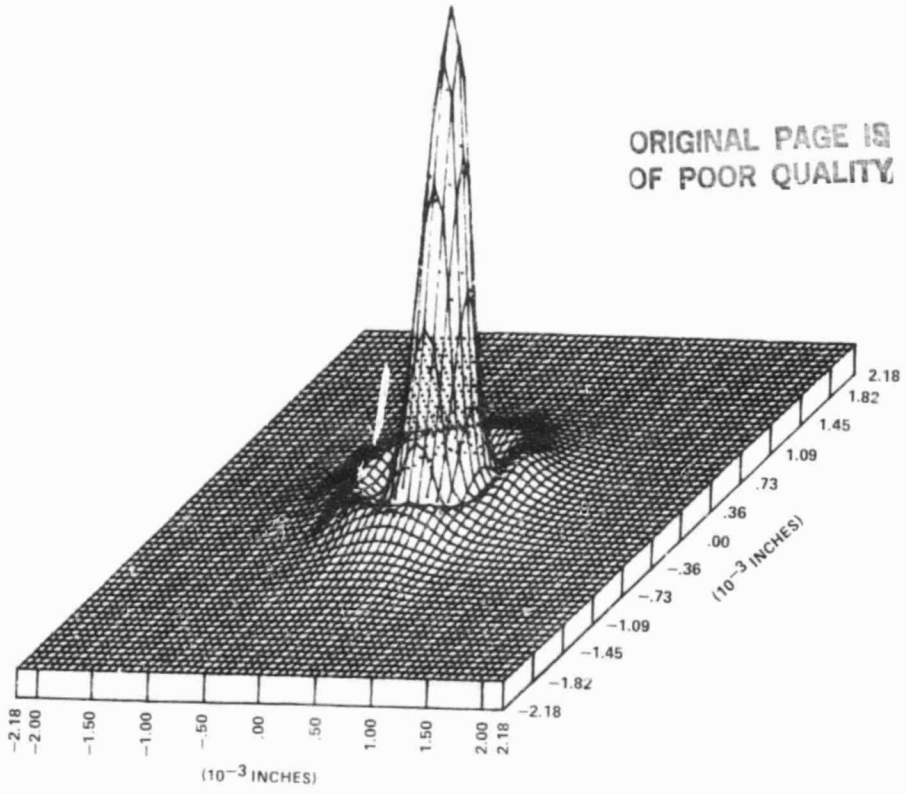

Figure 6c. Normalized PSF with $\lambda/40$ rms wavefront error, Rigel to S20.

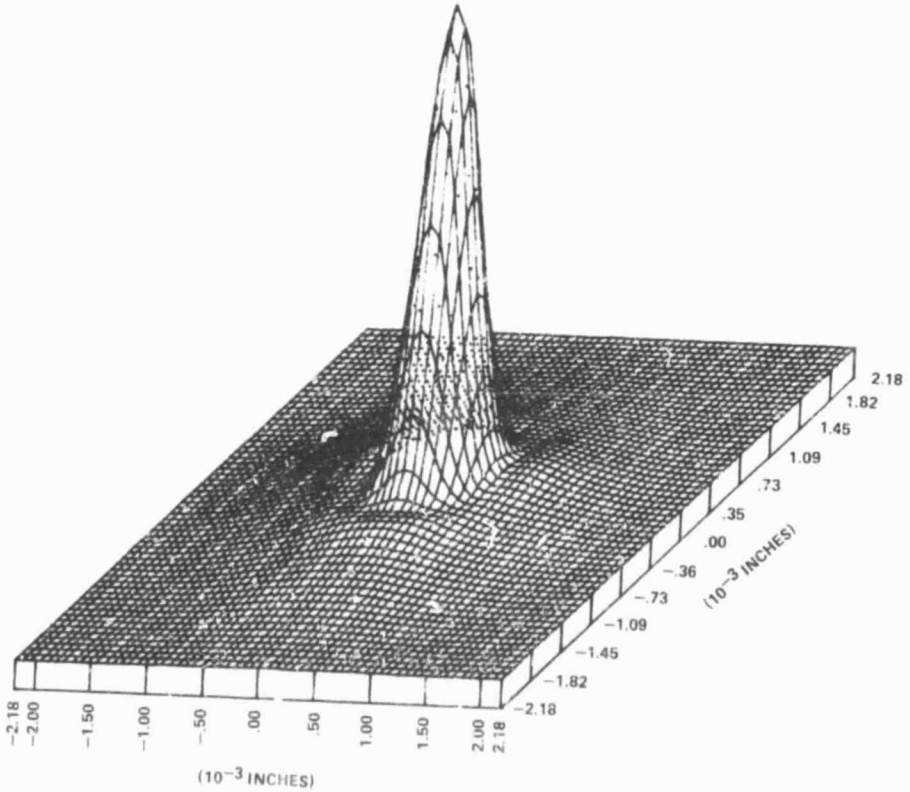

Figure 6d. Normalized PSF with $\lambda/40$ rms wavefront error, Rigel to CID.

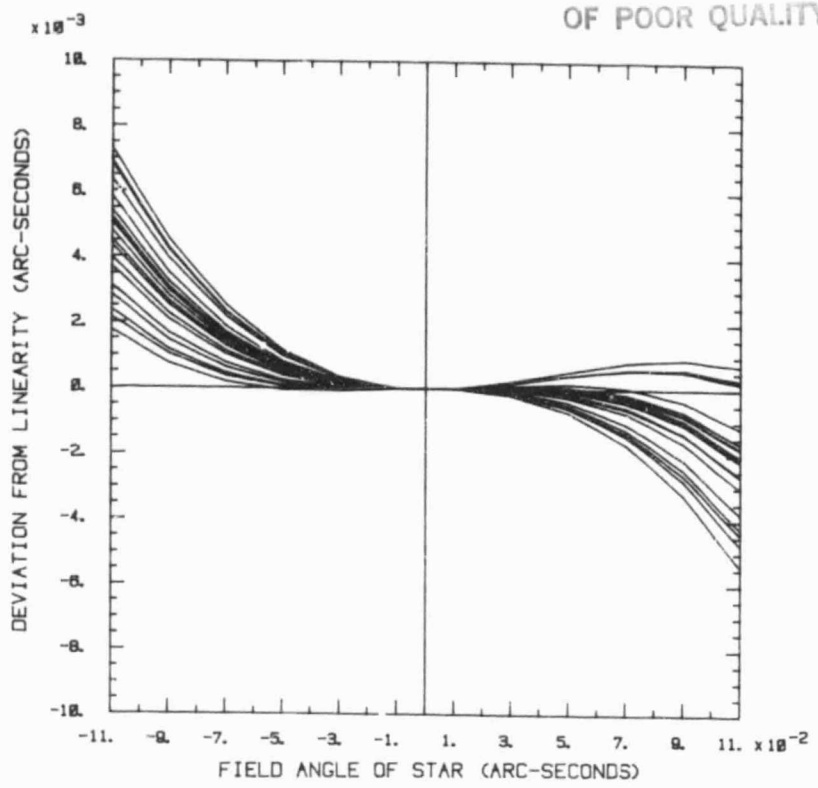

Figure 7a. Sample linearity deviations with $\lambda/20$ rms wavefront error, Rigel to S20.

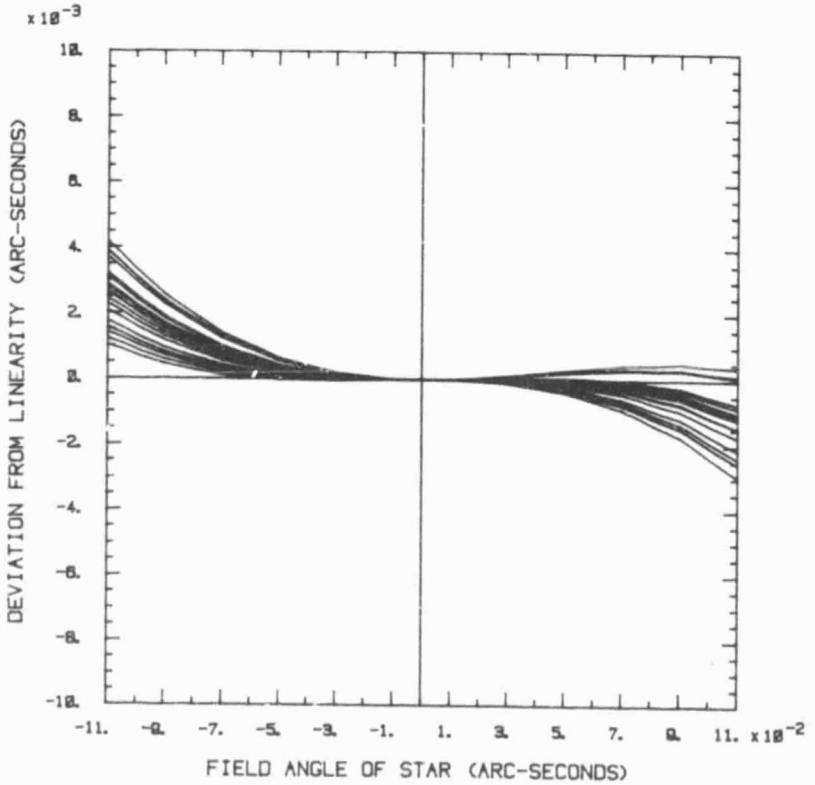

Figure 7b. Sample linearity deviations with $\lambda/20$ rms wavefront error, Rigel to CID.

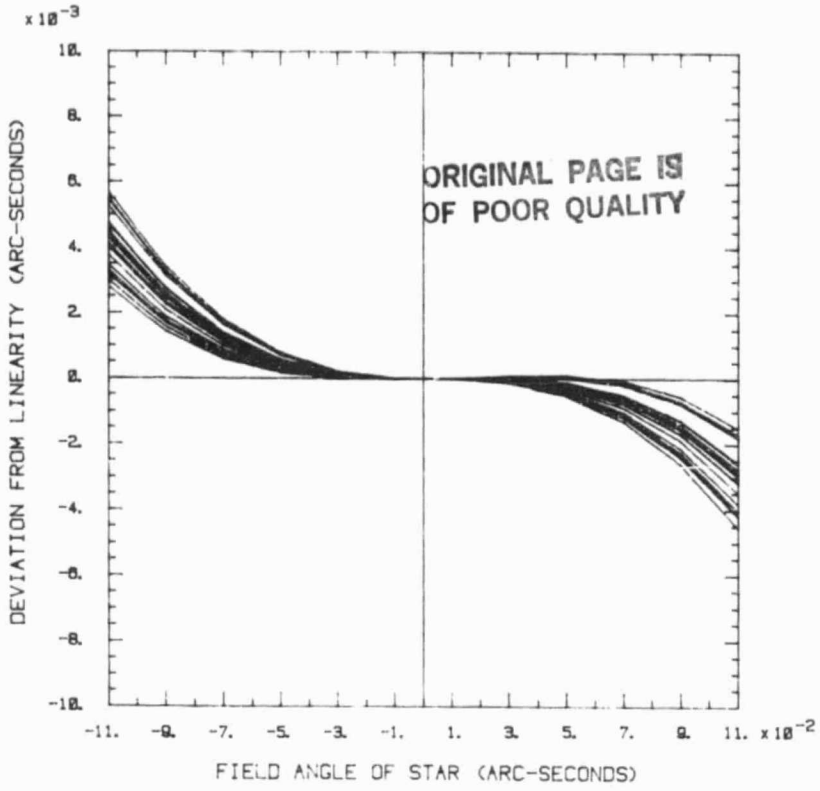

Figure 7c. Sample linearity deviations with $\lambda/40$ rms wavefront error, Rigel to S20.

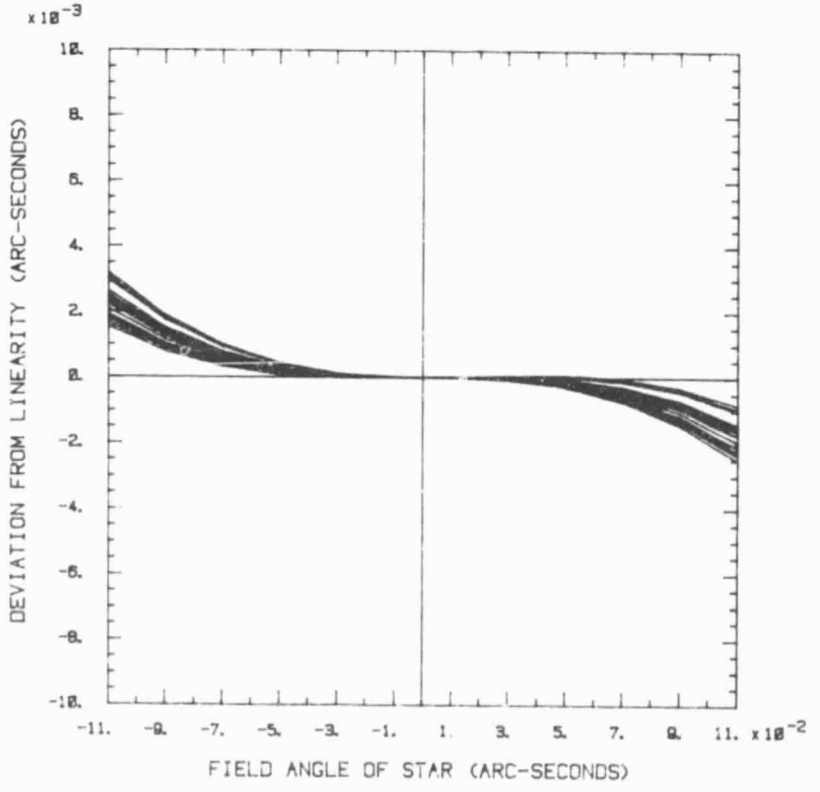

Figure 7d. Sample linearity deviations with $\lambda/40$ rms wavefront error, Rigel to CID.

C. Sensitivity of Maximum Linearity Deviation and Focal Position to Other Fabrication Errors

Fabrication errors involving the optical elements' positions, orientations, and curvatures may significantly change the PSF shape and the focal position. Lateral shifts, axial shifts, and tilts of 0.01 in., 0.001 in., and 10 arc-sec, respectively, were tried. Also, radii of curvature changes of 0.002 in., 0.01 in., and 0.01 in. were applied to the primary, secondary, and tertiary mirrors, respectively. Tables 3 and 4 show the significant changes. Compare these values with those in Table 2. The linearity deviation curve appears to be more sensitive to random wavefront error.

TABLE 3. MAXIMUM LINEARITY DEVIATIONS WITH CHANGES IN OPTICAL ELEMENTS.[a,b] (UNITS: MILLIARC-SEC)

	Range	(Lateral Shift) (of 0.01 in.) S20	CID	(Tilt by) (10 arc-sec) S20	CID
Corrector	± 50	0.73	0.39	0.73	0.46
Surface	±110	5.52	3.05	5.20	3.26
Secondary	± 50	0.55	0.30	0.42	0.23
Mirror	±110	4.70	2.59	4.05	2.24
Tertiary	± 50	0.52	0.28	(negligible change)	
Mirror	±110	4.52	2.49		

a. Other changes had negligible effect (see text).

b. Image divider was moved to new geometrical best focus.

TABLE 4. MAGNITUDE OF FOCAL POINT SHIFTS FROM NOMINAL VALUES UNITS: (0.001 in.)

	Lateral Shift of 0.01 in.	Axial Shift by 0.001 in.	Vary Radii of Curvature[a]	Tilt by 10 arc-sec
Corrector	(a)[b] 0.1	—	—	0.0
Surface	(r)[c] 0.0	—	—	3.4
Primary	(a) 0.4	42.6	42.6	0.0
Mirror	(r) 65.1	0.0	0.0	14.5
Secondary	(a) 0.1	63.2	20.0	0.0
Mirror	(r) 19.9	0.0	0.0	6.8
Tertiary	(a) 0.2	20.4	62.2	0.0
Mirror	(r) 35.1	0.0	0.0	1.4

a. Change primary, secondary, and tertiary by 0.002, 0.01, and 0.01 in., respectively.

b. Axial direction.

c. Radial or lateral direction.

VI. METHODS FOR INCREASING THE LINEARITY OF THE OUTPUT SIGNAL

A. Defocus

In order to test the effect of defocus on the output linearity, the dividing edge was moved 0.1 in. behind the focus (Table 1). For the S20 detector, the linearity deviations at ±50 and ±110 milliarc-sec were decreased from 0.35 and 3.71 milliarc-sec to 0.08 and 0.85 milliarc-sec, respectively. For the CID version the deviations at ±50 and ±110 milliarc-sec were reduced from 0.19 and 2.06 milliarc-sec to 0.09 and 1.01 milliarc-sec, respectively. Thus, defocussing has decreased the linearity deviations in the ideal telescope and has made the difference between the S20 and CID detector options smaller in this respect. However, the noise equivalent angles are increased by factors of 4 and 2 for the S20 and CID options, respectively.

B. Scaling of Output Signal

Up to this point in the analysis, the output signal was scaled by the slope of the raw output signal at the null point. If the signal is scaled such that there is zero deviation at e.g. 30 milliarc-sec, the deviations may be reduced near that angle. For the S20 this reduces the linearity deviations from 0.35 to 0.23 milliarc-sec at 50 milliarc-sec. For CID the linearity deviation to 50 milliarc-sec is reduced from 0.19 to 0.13 milliarc-sec. In both cases the deviation at ±110 milliarc-sec is not very much improved. If the scaling point is too high the deviation will be large for small angles. The noise equivalent angle is not significantly affected by this change in scaling.

VII. SUMMARY AND RECOMMENDATIONS

The results show that the ability of the star tracker to meet linearity requirements is extremely sensitive to optical element fabrication tolerances. Furthermore, under actual flight conditions the linearity would also depend on spacecraft attitude control, noise in control electronics, aging of materials, contamination of surfaces, mechanical stability, etc. The ability to meet the linearity requirements with a focused image will be enhanced by the following:

1) Use a detector with high quantum efficiency and large average wavelength.

2) Minimize random wavefront error.

Several other actions which may possibly increase the probability of success are:

1) Decrease the number of optical elements by eliminating the corrector plate and changing the mirror shapes to aspheres.

2) Defocus the image slightly to increase linearity. Watch the NEA and tolerances on aperture shapes while doing this!

3) Calibrate the output signal. The simplest type of calibration was mentioned in Section VI-B.

REFERENCES

1. Fairbank, W. M.; Everitt, C. W. F.; and DeBra, D. B.: Report on a Program to Develop a Gyro Test of General Relativity in a Satellite and Associated Control Technology. W. W. Hanson Laboratories of Physics and the Department of Aeronautics and Astronautics, Stanford University, Stanford, California, June 1980.

2. Jones, C. (private communication); see also: Kollodoge, J.: An Advanced Tracker Design for Pointing and Control of Space Vehicles Using the Charge Injection Device. American Astronautical Society 82-031; J. A. Hall, Arrays and Charge Coupled Devices, in Applied Optics and Optical Engineering, edited by R. R. Shannon and J. C. Wyant (Academic Press, New York, 1980), pp. 349-440.

3. Levi, L.: Handbook of Tables of Functions for Applied Optics, (CRC Press, Cleveland, Ohio, 1974).

4. For example: L. Motz and A. Duveen, Essentials of Astronomy, (Wadsworth Publishing Co., Belmont, California, 1966); C. W. Allen, Astrophysical Quantities, 3rd ed. (Athlone Press, London, 1973).

5. Brewer, S., POLYPAGOS: Polychromatic Program for the Analysis of General Optical Systems, Aerospace Corporation report No. TR-0059 (6311)-1, September 1970; R. V. Larson, POLYPAGOS User's Manual, Report No. TR-0172(2311)-1, October 1971; R. V. Larson, POLYANA User's Guide, Report No. TR-0074 (4407)-6, April 1974.